SPATIAL VARIATION IN LIQUEFACTION RISK

Gordon A. Fenton[1] and Erik H. Vanmarcke[2]

[1] Associate Professor, Dept. of Engineering Mathematics, DalTech, Dalhousie University, Halifax, Nova Scotia, B3J 2X4, phone: (902) 420-7726, FAX: (902) 423-1801, Email: gordon@random.field.tuns.ca

[2] Professor, Dept. of Civil Engineering and Operations Research, Princeton University, NJ 08544, Phone: (609) 258-5896, FAX: (609) 258-3791, Email: erikvm@soil.princeton.edu

SPATIAL VARIATION IN LIQUEFACTION RISK

Gordon A. Fenton and Erik H. Vanmarcke

Abstract

Basic concepts and methods of random field theory, useful for characterizing 'distributed disordered systems', are applied to a soil deposit to evaluate the spatial extent of liquefaction under typical conditions. The soil deposit, modeled after a site located at the Wildlife Management Area in California, is represented by a three-dimensional random properties field and is subjected to multiple realizations of a space-time random field of earthquake ground motion patterned after the Superstition Hills event of 1987. Based on Monte Carlo analysis using a deterministic one-dimensional nonlinear finite element program, spatial variability of liquefaction risk is assessed and techniques for improving estimates of liquefaction risk, accounting for local spatial variation, are investigated.

Keywords

liquefaction, numerical modelling and analysis, statistical analysis

1. INTRODUCTION

In probabilistic soil profile modelling, material characteristics are modeled as random functions; $U(\underset{\sim}{x})$ representing the value of a soil property at spatial location $\underset{\sim}{x}$. In practice, one needs to obtain a best estimate of the property, along with data on its variability and spatial correlation. Data on variability (e.g. Lumb, 1966, Schultze, 1971, and Singh, 1970) and spatial dependence (e.g. DeGroot *et al.*, 1993, Chiasson *et al.*, 1995, Asaoka *et al.*, 1982) are generally very limited and this information tends to be quite site specific.

Geotechnical performance often depends on maxima or minima of some spatially averaged material property or response measure (Vanmarcke, 1977). In particular, under earthquake shaking, liquefaction-induced failure can occur only if the resistance to seismic stresses is sufficiently low over a sufficiently large volume of foundation soil; high liquefaction potential need not be a problem if confined to small, isolated volumes, as demonstrated in a liquefaction stability analysis by Hryciw *et al.* (1990). Thus, studies of liquefaction risk at a site should consider not only the liquefaction potential at sample points, as traditionally done, but also the spatial variation of liquefaction potential over the entire site.

Because of the highly nonlinear nature of liquefaction response of a soil mass, the spatial distribution of liquefied regions can be most accurately obtained through multiple simulation runs, i.e. through a so-called Monte Carlo analysis. A first order-second moment approach – involving linearization of the relations between the response and input – often leads to large errors in highly nonlinear systems when the material properties show high variability, as is common for soils. In Monte Carlo simulation, the challenge is to simulate sets of properly correlated finite-element local averages; each set of simulated values serves as input into (multiple) deterministic finite element analysis. Sample statistics of response parameters can then be computed.

An appropriate soil model for stochastic finite element analysis involves a partition of the soil volume into a set of finite elements. A vector of material properties, drawn from realizations of three-dimensional local-average random fields, is then associated with each element. In the simulation, one must account for 'point variance' reduction and correlation between elements, consistent with the dimensions of the finite elements and the correlation parameters of the underlying fields. The variance function, which reflects the amount of variance reduction due to local averaging and depends on one or more scales of fluctuation, frugally captures the correlation structure, and is well suited for the simulation of local averages (Vanmarcke, 1984).

Although the soil properties are being modeled by a three-dimensional random field, the liquefaction analysis will be carried out using only a one-dimensional finite element program applied to one column of the soil mass at a time. This considerable simplification of the problem is necessitated by the enormous computational requirements of a non-linear, time-stepping, stochastic (Monte Carlo) analysis. In addition, and again partly due to computational time issues but also due to the one-dimensional sequential approximation to a three-dimensional problem, the paper considers only the *initiation* of liquefaction. While it is well known that post-event pore pressure redistribution is important in liquefaction, it is not felt that a 1-D model will properly reflect this redistribution since in the 1-D model almost all shear wave motion is absorbed by the liquefied layer and the surface ceases to move. On the shorter time scale of the event itself, the initiation of liquefaction in the soil is believed to be modeled reasonably accurately via one-dimensional approximations. The paper concentrates on the spatial variation, over a horizontal plane, of the initial liquefaction state. A picture of the initial liquefaction state is built up by looking at horizontal cross-sections through the collection of one-dimensional soil columns making up the soil mass.

2. MODEL SITE: SOIL LIQUEFACTION

An earthquake of magnitude M_s = 6.0, on April 26, 1981 in the Imperial Valley near Westmorland, California, caused significant damage, in many cases through liquefaction. This prompted a detailed geological survey of the valley, including the installation of accelerometers and piezometers to record ground motions and changes in pore-water pressure during future earthquakes at the Wildlife Management Area. The Wildlife Management Area is located 3 km south of Calipatria in the Imperial Wildfowl Management Area, lying on the west side of the incised flood plain of the Alamo River.

The site was instrumented in 1982 with surface and down-hole (7.5 m depth) accelerometers and 6 pore-water pressure transducers (Bennett *et al.*, 1984). The Superstition Hills event (M_s = 6.6), recorded in 1987 (Holzer *et al.*, 1988), resulted in liquefaction at the site in the form of sand boils and limited lateral spreading and motivates this study – the following model is based on the Wildlife site.

Within the upper three geological units, a closer examination by Holzer *et al.* revealed five soil strata to the level of the down-hole accelerometer;

1) Layer 1 (0.0 to 1.2 m): very loose silt,
2) Layer 2 (1.2 to 2.5 m): very loose silt,
3) Layer 3 (2.5 to 3.5 m): very loose to loose sandy silt,
4) Layer 4 (3.5 to 6.8 m): loose to medium dense silty sand, and
5) Layer 5 (6.8 to 7.5 m): medium to stiff clayey silt.

The water table at a depth of 1.2 m forms the boundary between Layers 1 and 2.

The random medium representation of the soil properties and deterministic finite element program used to assess the spatial variation of liquefaction at the model site are described in the following sections. Recognizing that little information concerning spatial variability of the soil properties at the site is available, the model requires many parameters to be assumed using reasonable estimates. Since many of these statistical parameters were not verified at the Wildlife site, this example serves primarily to investigate the degree of spatial variability in liquefaction under reasonable assumptions and to investigate techniques of evaluating liquefaction risk in the presence of spatial variability. The intensity of the earthquake excitation and the scales of fluctuation of the soil properties were varied for the purpose of sensitivity analysis.

The soil volume to be modeled is 80 $\times$ 80 m laterally by 7.5 m in depth and is partitioned into a 16 $\times$ 16 $\times$ 32 set of finite elements. Thus each element has dimensions 5 $\times$ 5 m laterally by 0.23 m vertically. Realizations of the random soil properties within each element are obtained by column-wise extraction from a set of 3-D local-average simulations.

2.1 Stochastic Soil Model

For this study, the soil parameters expected to have the greatest impact on site response and liquefaction likelihood and selected to be modeled as 3-D random fields were: permeability (k), porosity (n), modulus of elasticity (solid phase) (E), Poisson's ratio (solid phase) (ν), and dilation reference angle (Φ). The ratio of Φ to the friction angle determines whether initial contraction is followed by dilation or contraction in the soil during shaking. All of these properties, and in particular the dilation reference angle, are generally found through laboratory tests on soil samples. These parameters are required as input to the finite element analysis program to be discussed later. Their treatment and precise interpretation within the finite element algorithm is discussed in detail by Prevost (1989). Permeability and, indirectly, porosity, are perhaps the most important parameters influencing liquefaction in sandy soils. Water trapped within the soil structure carries an increasing fraction of the stress as the soil densifies during shaking. Eventually the inter-granular stresses may become so low that relative movement between particles becomes possible and the medium effectively liquefies.

Beyond CPT tests performed at a small number of locations, the published site information (Bennett *et al.*, 1984, and Holzer *et al.*, 1988) contains barely enough data to establish mean parameters as estimated by Keane *et al.* (1989) and listed in Table 1 as a function of depth. Estimates of the statistical nature of the above parameters are based on a combination of engineering judgement and a review of the literature (Fenton, 1990). Assumed variances associated with each parameter are also shown in Table 1 as a function of depth.

In all cases the random material parameters are obtained by transforming a 3-D zero-mean unit-variance homogeneous Gaussian field, $Z(\underset{\sim}{x})$, realizations of which are produced using the three-dimensional Local Average Subdivision (LAS) method (Fenton and Vanmarcke, 1990). Letting $U_i(\underset{\sim}{x})$ represent the value of the i'th soil property at the spatial point $\underset{\sim}{x} = \{x, y, z\}^T$, with z the depth below the surface,

$$U_i(\underset{\sim}{x}) = \mathcal{T}_i\Big(\mu_i(z) + \sigma_i(z)\, Z_i(\underset{\sim}{x})\Big), \tag{1}$$

where $\mu_i(z)$ is the mean, $\sigma_i(z)$ is the standard deviation, and $\mathcal{T}_i$ is a transformation taking the Gaussian process, $Z_i(\underset{\sim}{x})$, into the marginal distribution appropriate for property i. Notice that the formulation allows trends in the mean and variance as a function of depth to be incorporated.

For the permeability, elastic modulus, and dilation reference angle, all assumed to be lognormally distributed, the transformation $\mathcal{T}_i$ is the exponential

$$U_i(\underset{\sim}{x}) = \exp\left\{\mu_{\ln i}(z) + \sigma_{\ln i}(z)\, Z_i(\underset{\sim}{x})\right\}. \tag{2}$$

Table 1. Average soil properties and associated parameters of the underlying Gaussian fields.

Property	Depth (m)	0 – 1.2	1.2 – 2.5	2.5 – 3.5	3.5 – 6.8	6.8 – 7.5
Permeability ($k, m/s$)	mean	1×10^{-5}	1×10^{-5}	1×10^{-5}	1×10^{-4}	1×10^{-6}
	$\mu_{\ln k}$	-11.7	-11.7	-11.9	-9.7	-14.1
	$\sigma^2_{\ln k}$	0.6	0.6	0.8	1.0	0.5
Porosity[1] (n)	mean	0.42	0.42	0.42	0.42	0.42
	$\mu_{n'}$	0	0	0	0	0
	$\sigma^2_{n'}$	1.0	1.0	1.0	1.0	1.0
Elastic Modulus ($E, N/m^2$)	mean	3.9×10^{7}	3.7×10^{7}	5.4×10^{7}	5.4×10^{7}	7.0×10^{7}
	$\mu_{\ln E}$	17.1	17.1	17.4	17.2	17.7
	$\sigma^2_{\ln E}$	0.8	0.6	0.8	1.2	0.8
Poisson's[2] ratio (ν)	mean	0.275	0.275	0.275	0.275	0.275
	$\mu_{\nu'}$	0	0	0	0	0
	$\sigma^2_{\nu'}$	1.0	1.0	1.0	1.0	1.0
Dilation Reference Angle (Φ)	mean	21.3°	20.0°	19.0°	18.0°	5.0°
	$\mu_{\ln \Phi}$	2.95	2.90	2.84	2.77	1.51
	$\sigma^2_{\ln \Phi}$	0.2	0.2	0.2	0.3	0.2

[1] see Eqs. 4 and 5
[2] see Eqs. 7 and 8

Porosity is related to both permeability and soil relative density, the latter of which is also related to the initial vertical stresses in the medium as well as the shear wave velocities. The porosity at the Wildlife site is assumed to have a constant mean of 0.42. Recognizing that n must be bounded, the following transformation $\mathcal{T}_n$ (see Eq. 1) changes a normally distributed variate into a bounded distribution:

[3] $$U_n = a + (b-a)\mathcal{T}_n(Y) = a + \frac{b-a}{2}\left\{1 + \tanh\left(\frac{Y}{2\pi}\right)\right\},$$

which is a one-to-one mapping of $Y \in (-\infty, \infty)$ into $U_n \in (a, b)$, where Y is obtained from the random field Z according to Eq. 1

[4] $$Y(\underset{\sim}{x}) = \mu_{n'}(z) + \sigma_{n'}(z)\, Z_{n'}(\underset{\sim}{x}).$$

where $\mu_{n'}$ and $\sigma_{n'}$ are the mean and standard deviation of Y, which can be obtained in practice by taking the first two moments of the inverse

[5] $$Y = \mathcal{T}_n^{-1}\left(\frac{U_n - a}{b-a}\right) = \pi \ln\left(\frac{U_n - a}{b - U_n}\right)$$

Other than a simple means of transforming an unbounded distribution to a bounded distribution, Eq. (3) has no physical basis. There is insufficient data to either verify or discount its use, and so it should be viewed simply as an approximation to allow the stochastic treatment of bounded random soil parameters. Depending on the value of $\sigma_{n'}(z)$ selected for use in Eq. (4), the marginal

distribution of U_n follows a variety of symmetric shapes. For $\mu_{n'} = 0$, the marginal distribution of U_n is given by

$$[6] \qquad f_{U_n}(u) = \frac{(b-a)\sqrt{\frac{\pi}{2}}}{(u-a)(b-u)\sigma_{n'}} \exp\left\{ -\frac{1}{2}\left(\frac{\pi \ln\left(\frac{u-a}{b-u}\right)}{\sigma_{n'}} \right)^2 \right\}$$

For the assumed value of $\sigma^2_{n'} = 1.0$ used herein (see Table 1), the distribution of U_n is bell shaped with mode at the midpoint, $\frac{1}{2}(b + a)$. In this case study, it is assumed that $n \in (0.22, 0.62)$ with mean 0.42. While this may seem to be a fairly wide range on the porosity, it should be noted that the distribution given by Eq. (6) implies that 90% of porosity realizations lie between 0.37 and 0.47. The solid phase (soil) mass density, ρ_s, was taken to be 2687 kg/m^3 (Keane *et al.*, 1989) giving a mean soil dry unit mass of $(1 - 0.42)(2687) = 1558\ kg/m^3$.

Because it is well known that soil porosity is related to permeability, the underlying Gaussian fields $Z_{n'}$ and $Z_{\ln k}$ are generated so as to be mutually correlated on a point-by-point basis. This is accomplished by generating two independent random fields and then linearly combining them using the Cholesky decomposition of the 2×2 cross-correlation matrix to yield two properly correlation random fields (Fenton, 1994). A correlation coefficient of 0.5 is assumed, however it must be recognized that the true correlation between these properties is likely to be quite variable and site specific. Although the other random soil properties are also felt to be correlated with soil porosity, their degree of correlation is significantly less certain than in the case of permeability, which is already somewhat speculative. For this reason, the other random properties are assumed to be independent. Recalling that the introduction of correlation decreases the variability between pairs of random variables, the assumption of independence increases the overall variability contained in the model. Thus, it is deemed better to assume independence than to assume an erroneous correlation. The effect of cross-correlation between, say, porosity and the dilation reference angle on the spatial distribution of liquefaction is left an open question that may be better left until more is known about the statistical correlations between these properties.

Poisson's ratio is also chosen to be a bounded random variable, $\nu \in (0.075, 0.475)$, according to Eq. 3 with constant mean 0.275. Now Y is given by

$$[7] \qquad Y(\underset{\sim}{x}) = \mu_{\nu'}(z) + \sigma_{\nu'}(z)\, Z_{\nu'}(\underset{\sim}{x}),$$

so that

$$[8] \qquad U_\nu = 0.075 + 0.4\,\mathcal{T}_\nu(Y),$$

and the transformation $\mathcal{T}_\nu$ is the same as $\mathcal{T}_n$ in Eq. 3. Under this transformation, with $\sigma_{\nu'} = 1$, 90% of realizations of Poisson's ratio will lie between 0.24 and 0.31.

The relationship between the dilation reference angle, Φ, and the friction angle at failure, ϕ, as interpreted internally by the finite element analysis program, determines whether the soil subsequently dilates or contracts upon shaking. If the ratio Φ/ϕ exceeds 1.0, then only contraction occurs, otherwise initial contraction is followed by dilation. Since contraction results in increasing pore water pressure, this ratio is of considerable importance in a liquefaction analysis. Rather than considering both the dilation and friction angles to be random, only the dilation angle was selected as random; the friction angle was prescribed deterministically with $\phi = 21^o$ in Layer 1, 20^o in Layer

2, 22^o in Layers 3 and 4, and 35^o in Layer 5, as estimated by Keane and Prevost (1989). These assumptions still lead to the ratio Φ/ϕ being random.

The covariance function, $B(\underset{\sim}{\tau})$, used to model the spatial variability of all the random soil properties is of a simple exponential form parameterized by θ_v and θ_h, the scales of fluctuation in the vertical and horizontal directions respectively,

$$[9] \qquad B(\tau_1, \tau_2, \tau_3) = \sigma^2 \exp\left\{ -\frac{2}{\theta_h}\left(\sqrt{\tau_1^2 + \tau_2^2}\right) - \frac{2|\tau_3|}{\theta_v} \right\},$$

where $\underset{\sim}{\tau} = \{\tau_1, \tau_2, \tau_3\}^T = \underset{\sim}{x} - \underset{\sim}{x}'$ denotes the separation distance between two spatial points, $\underset{\sim}{x}$ and $\underset{\sim}{x}'$. Note that Eq. (9) has a partially separable form in τ_3 (vertically). This covariance function governs the underlying Gaussian random fields; after transformation into the desired marginal distributions, the covariance structure is also transformed so that comparison between statistics derived from real data and Eq. (9) must be made with caution. From the point of view of estimation, the statistical parameters governing the underlying Gaussian fields can always be simply obtained by performing an inverse transformation on the data prior to estimating the statistics. For example, if the parameter is treated as a lognormally distributed random process by transforming a normally distributed random field using the relationship $U = \exp\{Y\}$, then the corresponding mean, variance, and scale of fluctuation of Y can be found from the raw data by taking the logarithm of the data prior to statistical analysis. In the absence of spatial data, the following discussion is derived from the literature and is assumed to apply to the underlying Gaussian fields directly.

In the vertical direction, de Marsily (1985) proposes that the scale of fluctuation of soil permeability is of the order of 1 m and so $\theta_v = 1\ m$ is adopted here. The horizontal scale of fluctuation, θ_h, is highly dependent on the horizontal extent and continuity of soil layers. The USGS survey (Bennett *et al.*, 1984) indicated that the layers at the Wildlife site are fairly uniform and a ratio of horizontal to vertical scales $\theta_h/\theta_v \simeq 40$ was selected implying $\theta_h \simeq 40\ m$; this is in the same range as Vanmarcke's (1977) estimate of 55 m for the compressibility index of a sand layer. Although compressibility and permeability are of course different engineering properties, one might argue that the scale of fluctuation depends largely on the geological processes of transport of raw materials, layer deposition, and common weathering rather than on the actual property studied. Based on this reasoning, all the random soil properties are modeled using the same scales of fluctuation as well as the same form of the covariance function.

The simulations are repeated using a larger vertical scale, $\theta_v = 4\ m$, while holding the ratio of horizontal to vertical scales constant at 40. In the following, only the vertical scale of fluctuation is referred to when indicating the case studied.

2.2 Stochastic Earthquake Model

Earthquake ground motions vary from point to point in both time and space. Techniques have been developed to generate such fields of motion (Vanmarcke *et al.*, 1993), while studies of earthquake motions over arrays of seismometers provide estimates of the space-time correlation structure of ground motion (e.g. Boissières and Vanmarcke, 1995). Input earthquake motions in this study, applied to the base of the soil model on a point-wise basis, are realizations of a space-time random field with the following assumed space-frequency correlation function,

$$[10] \qquad \rho(\omega, \underset{\sim}{\tau}) = \exp\left\{ -\frac{\omega|\underset{\sim}{\tau}|}{2\pi cs} \right\},$$

where $\underset{\sim}{\tau} = \underset{\sim}{x} - \underset{\sim}{x}'$ is the lag vector between spatial points $\underset{\sim}{x}$ and $\underset{\sim}{x}'$, ω is the wave-component frequency (rad/sec), c is the shear wave velocity (taken as 130 m/sec at the base of the soil model), and s = 5.0 is a dimensionless parameter controlling the correlation decay.

Only one component of motion is used, modeled after the North-South component of the Superstition Hills event. Analyses by Keane and Prevost (1989) indicate that including the East-West and vertical components makes little difference to the computed (deterministic) site response (the North-South component had dominant amplitudes), and using it alone, Keane obtains remarkably good agreement with the recorded site response.

The marginal spectral density function, $G(\omega)$, governing the input motion spectral content was derived from the dominant NS component of earthquake acceleration, shown in Figure 1, recorded at the down-hole accelerometer for the Superstition Hills event. To reduce the number of time steps in the analysis, only 20.48 seconds of motion were generated – 1024 time steps at 0.02 seconds each. Using the Maximum Entropy method, a pseudo-evolutionary spectral density function was estimated in 4 consecutive time windows, starting at 7 seconds into the recorded acceleration as denoted by dashed lines in Figure 1. The derived spectral density functions shown in Figure 2, one for each time window, were then used to produce non-stationary earthquake acceleration realizations. The last $G(\omega)$ was actually based on the entire trailing portion of the recorded motion.

Admittedly, the down-hole motions include both upward propagating energy and downward propagating reflected energy, the latter of which is modified by existing material properties in the soil above the recording point. However, only the spectral density function of the down-hole motion is used to control the generated motions, not the detailed recordings themselves. The resulting simulations can be thought of as having a mean which includes the *mean* soil properties in the overlying field.

Figure 3 shows a realization of the input acceleration field sampled at two points separated by 80 m. Although the motions are quite similar, they are not identical and may be considered representative of the possible base motion at the site. The same marginal spectral density function was used at all spatial points over the base of the soil model, presumably reflecting the filtering of bedrock motion typical at the site. To partially assess the effect of earthquake intensity on the spatial distribution of liquefaction at the site, the study was repeated using the first set of artificial motions scaled by a factor of 0.7.

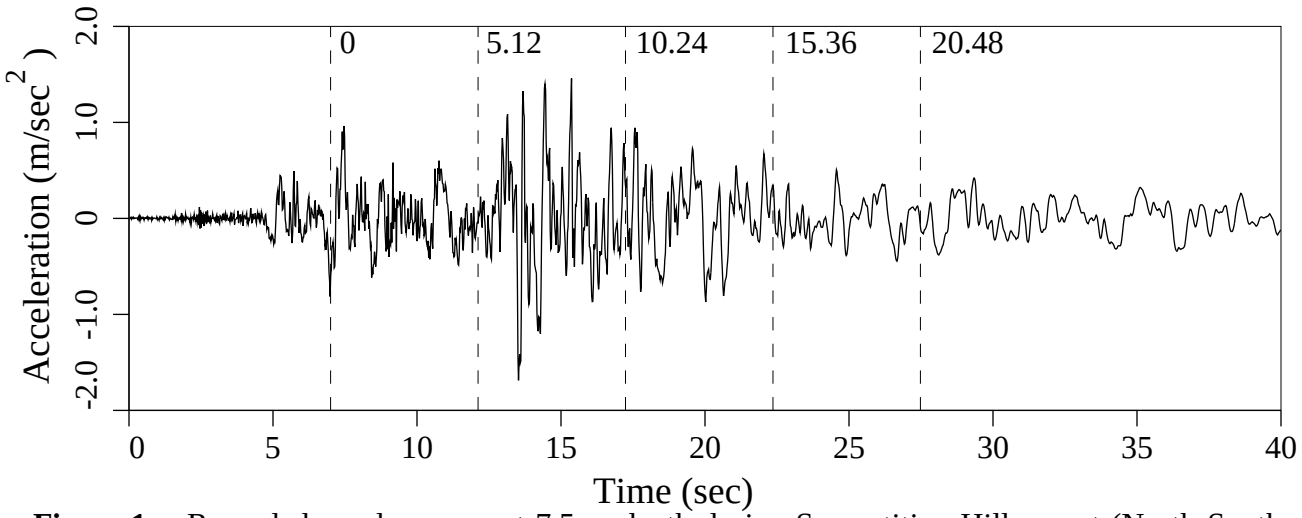

Figure 1. Recorded accelerogram at 7.5 m depth during Superstition Hills event (North-South component).

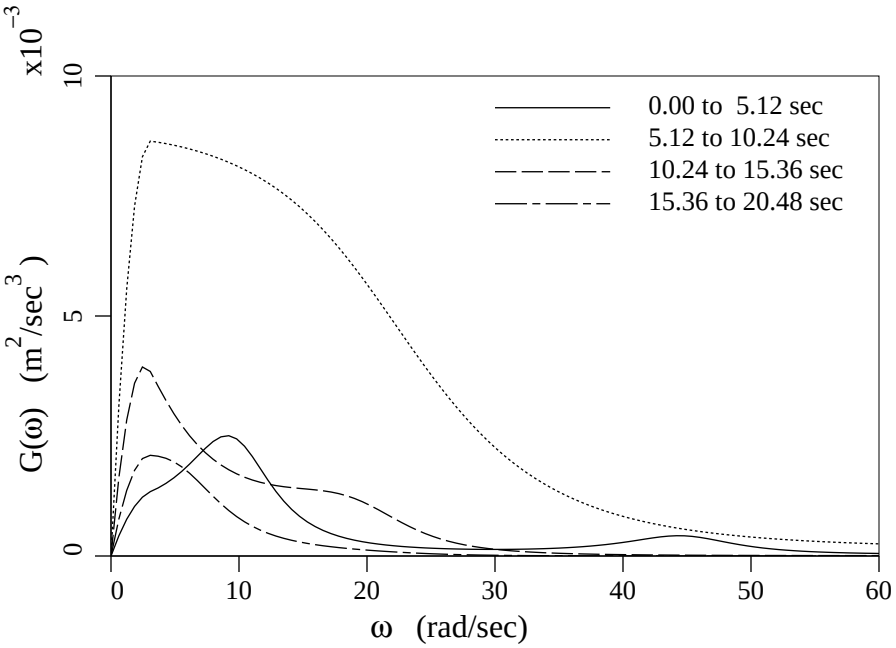

Figure 2. Pseudo-evolutionary spectral density function estimated from Superstition Hills event (North-South component) for four consecutive time windows.

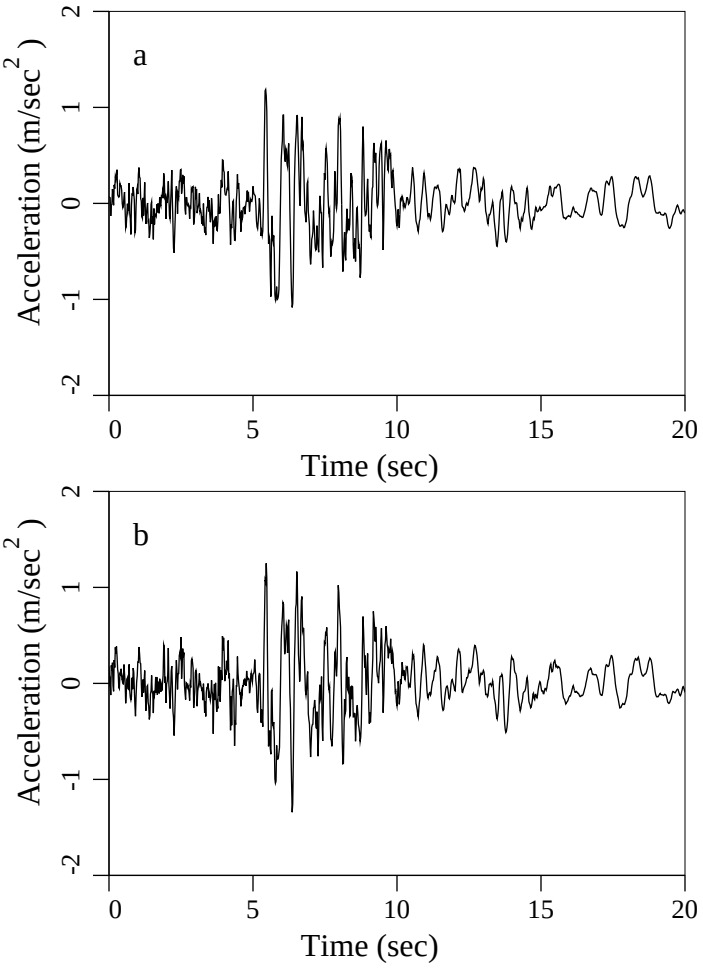

Figure 3. Sample acceleration records generated at two points, a and b, separated by 80 m.

2.3 Finite Element Model

The soil mass is divided into 256 columns arranged on a 16 $\times$ 16 grid, each column consisting of 32 elements (33 nodes) vertically. Realizations of the soil mass are excited by artificial earthquake motions applied at the base of each soil column and analyzed using DYNA1D, a one-dimensional nonlinear finite element model developed by Prevost (1989). DYNA1D employs multiple yield level elasto-plastic constitutive theory to take into account the nonlinear, anisotropic, and hysteretic stress-strain behavior of the soil as well as the effects of the transient flow of pore water through the soil media and its contractive/dilative nature. Each finite element is assigned soil properties, either deterministic values or from realizations of random fields.

Soil columns are then analyzed individually by DYNA1D, so that 256 invocations of DYNA1D are required for each realization of the soil mass. The column analyses are independent and the only link between the soil columns is through their correlated properties. It is unknown how the coupling between columns in a fully three-dimensional dynamic analysis would affect the determination of global liquefaction potential, however it is believed that the analysis proposed herein represents a

reasonable approximation to the fully three-dimensional analysis at this time, particularly since the site is reasonably level and only liquefaction initiation is considered.

The surface response obtained from the DYNA1D analysis of a single column of soil is shown in Figure 4 along with a typical realization of the input motion acting at the column base. The soil at a depth of about 2.7 m began to liquefy after about 10 seconds of motion. This is characterized at the surface by a dramatic reduction in response as the liquefied layer absorbs the shear wave motion propagating from below.

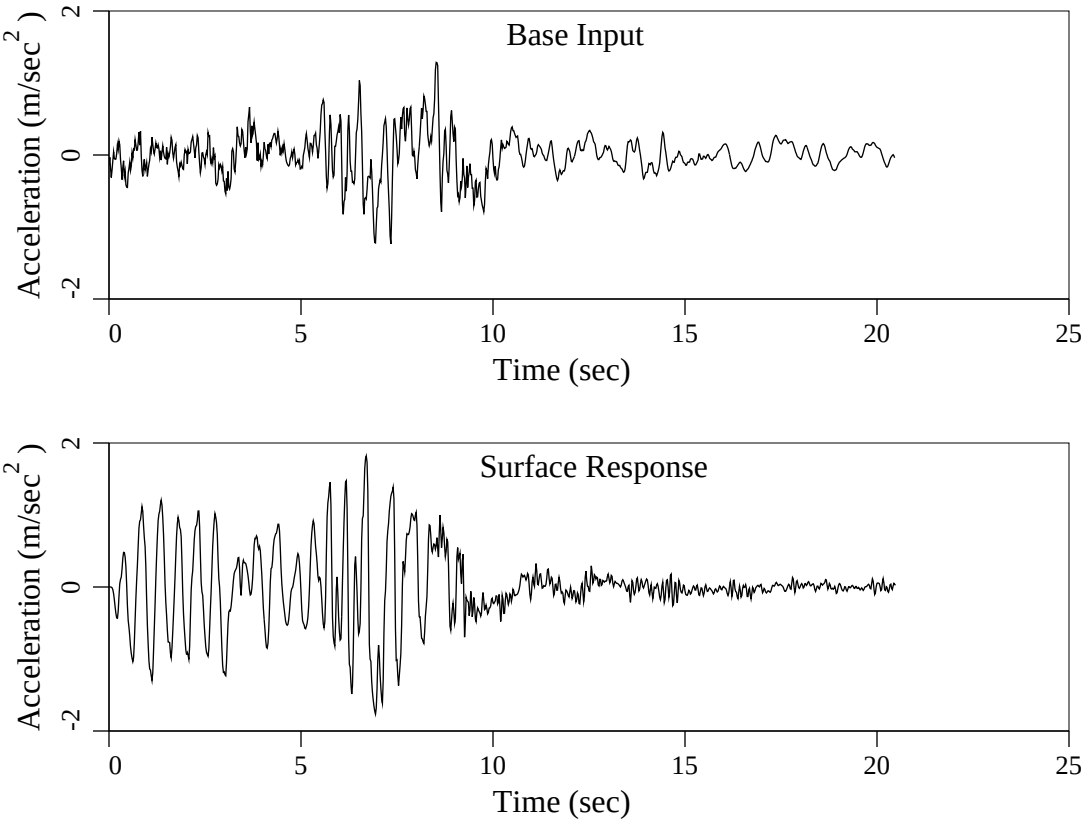

Figure 4. Base input and surface response computed by DYNA1D for a particular soil column realization.

Of particular interest in the evaluation of liquefaction potential at the site is the prediction of surface displacement and pore water pressure buildup while shaking lasts. As the global analysis consists of a series of one-dimensional column analyses, it was decided not to use the surface displacement predictions as indicators of liquefaction potential. Rather, the pore pressure ratio associated with each element was selected as the liquefaction potential measure to be studied. Redistribution of pore water pressure after the earthquake excitation, which could lead to further liquefaction of upper soil layers, was not considered in this initial study.

2.4 Measures of Liquefaction

The finite element program calculates the excess pore water pressure, u_i, in each element i as a function of time. The ratio $q_i = u_i/\sigma'_{oi}$, where σ'_{oi} is the initial vertical effective stress in the i^{th} element, is commonly thought of as the parameter measuring the occurrence of liquefaction (Seed, 1979) and will be referred to herein as the *liquefaction index*. Note that, owing to the one-dimensional nature of the finite element analysis, the horizontal effective stress is ignored and liquefaction is based only on the initial vertical effective stress.

When q_i reaches a value of 1, the pore water is carrying the load so that soil particles become free to slip and liquefaction occurs. It is possible, however, for liquefaction to take place at values of q_i slightly less than 1, as it is only necessary that most of the lateral strength or bearing capacity is lost. Fardis *et al.* (Mar. 1982) suggest that the liquefied fraction of the i^{th} element of soil, η_i, be calculated as

$$\eta_i = \mathrm{P}\left[\frac{u_i}{\sigma'_{oi}} \geq 0.96\right] \tag{11}$$

for undrained and partially drained effective stress models. The probability P $[\cdot]$ on the right hand side can be evaluated through a sequence of simulations. Fardis then goes on to evaluate the risk of liquefaction, L, as the probability that the maximum of $\eta(z)$ over the depth z is close to 1,

$$L = \mathrm{P}\left[\max_z(\eta(z)) \approx 1\right] \tag{12}$$

where now $\eta(z)$ is interpreted, not as a probability, but rather as the sample liquefied fraction. For individual soil columns where interaction with adjacent soil is ignored, such an approach is reasonable since the occurrence of liquefaction at a given layer will result in the loss of lateral resistance at the surface. Shinozuka and Ohtomo (1989) have a slightly different approach involving summing the liquefaction indices q over depth to obtain the vertically averaged liquefaction index $\mathcal{Q}$,

$$\mathcal{Q} = \frac{1}{h}\int_0^h \frac{u(z)}{\sigma'_o(z)}\,dz, \tag{13}$$

where h is the total depth of the modeled column. In this way the effect of the vertical extent of a liquefied region can be incorporated into a risk analysis. But how important is the vertical extent of liquefaction? While it certainly has bearing on liquefaction risk, it is easy to imagine a situation in which a thin layer some distance below the surface becomes completely liquefied while adjoining layers above and below remain stable. Such a condition could yield a relatively low value of $\mathcal{Q}$ even though lateral stability at the surface may be lost. On the other hand, the vertical extent of liquefied regions may be more important to the occurrence of sand boils and vertical settlement. In that the risk of sand boils and/or vertical settlement is quantifiable using point or vertically averaged approaches, whereas the loss of lateral stability resulting in spreading or lateral movement depends on the spatial distribution of liquefaction, this study concentrates on the latter issue.

In the three-dimensional situation, neither approach discussed above is deemed entirely suitable. If the term 'global liquefaction' is used to denote the loss of lateral stability leading to large surface displacements at the site, then the occurrence of high q_i indices at an individual point (or small region) will not necessarily imply global liquefaction if adjacent regions retain sufficient strength.

Likewise if a particular layer is found to have high q values over a significant lateral extent, then global liquefaction risk could be high even though the average for the site may be low. In this study, the lateral spatial extent of liquefied regions is assumed to be the more important factor in the determination of global liquefaction risk for a site. For each realization, the analysis proceeds as follows

1) compute the liquefaction index $q_{ij}(t_\ell) = u_i/\sigma'_{oi}$ for each element i in the j^{th} column at each time step t_ℓ and repeat for all the columns,

2) compute the sum

$$Q_{i\ell} = \frac{1}{A}\sum_{j=1}^{n_c} q_{ij}(t_\ell)\Delta A_j$$

where A is the total area of the site model, ΔA_j is the area of the j^{th} column and n_c is the number of columns; $Q_{i\ell}$ is the i^{th} layer average liquefaction index at each time step t_ℓ.

3) determine the indices i^* and ℓ^* which maximize $Q_{i\ell}$. The index i^* now represents the depth of the plane with the maximum likelihood of liquefying at the time t_{ℓ^*} and $q_{i^*j}(t_{\ell^*})$ is the corresponding two-dimensional field of liquefaction indices (indexed by j).

4) determine the excursion area fraction defined by

$$A_q = \frac{1}{A}\sum_{j=1}^{n_c} I_A\Big(q_{i^*j}(t_{\ell^*}) - q\Big)\Delta A_j$$

for a variety of levels $q \in (0,1)$. The indicator function $I_A(\cdot)$ has value 1 for positive arguments and 0 otherwise.

Repeating the above steps for a number of realizations allows the estimation of the spatial statistics of the liquefaction indices q on the horizontal plane of maximum liquefaction likelihood. In particular, the excursion area fractions A_q are evaluated for $q = \{0.1, 0.2, \ldots, 0.9\}$.

Liquefaction of a column is defined as occurring when the liquefaction index q_i exceeds 0.96 in some element; the analysis of that column is then discontinued to save considerable computational effort and the liquefaction indices are subsequently held constant. In fact, numerical tests indicated that, at least under this one-dimensional model, the liquefied element absorbs most of the input motion (see Figure 4) so that little change was subsequently observed in the liquefaction indices of higher elements. The liquefied element can be considered the location of liquefaction initiation since post-event pore pressure redistribution is being ignored (and, in fact, is not accurately modeled with this one-dimensional simplification).

The horizontal plane having the highest average liquefaction index is found and the statistics of those indices determined. This plane will be referred to as the maximal plane. It is recognized that when liquefaction does take place it is not likely to be confined to a horizontal plane of a certain thickness. At the very least the plane could be inclined, but more likely liquefaction would follow a undulating surface. This level of sophistication is beyond the scope of this initial study, however, which is confined to the consideration of liquefaction occurring along horizontal planes arranged over depth.

Figure 5 illustrates two realizations of the maximal plane. Regions which have liquefied are shown in white. In both examples, a significant portion of the area has q indices exceeding 0.9 and there is clearly significant spatial variation. The grey scale representation was formed by linear interpolation from the 16×16 mesh of finite elements.

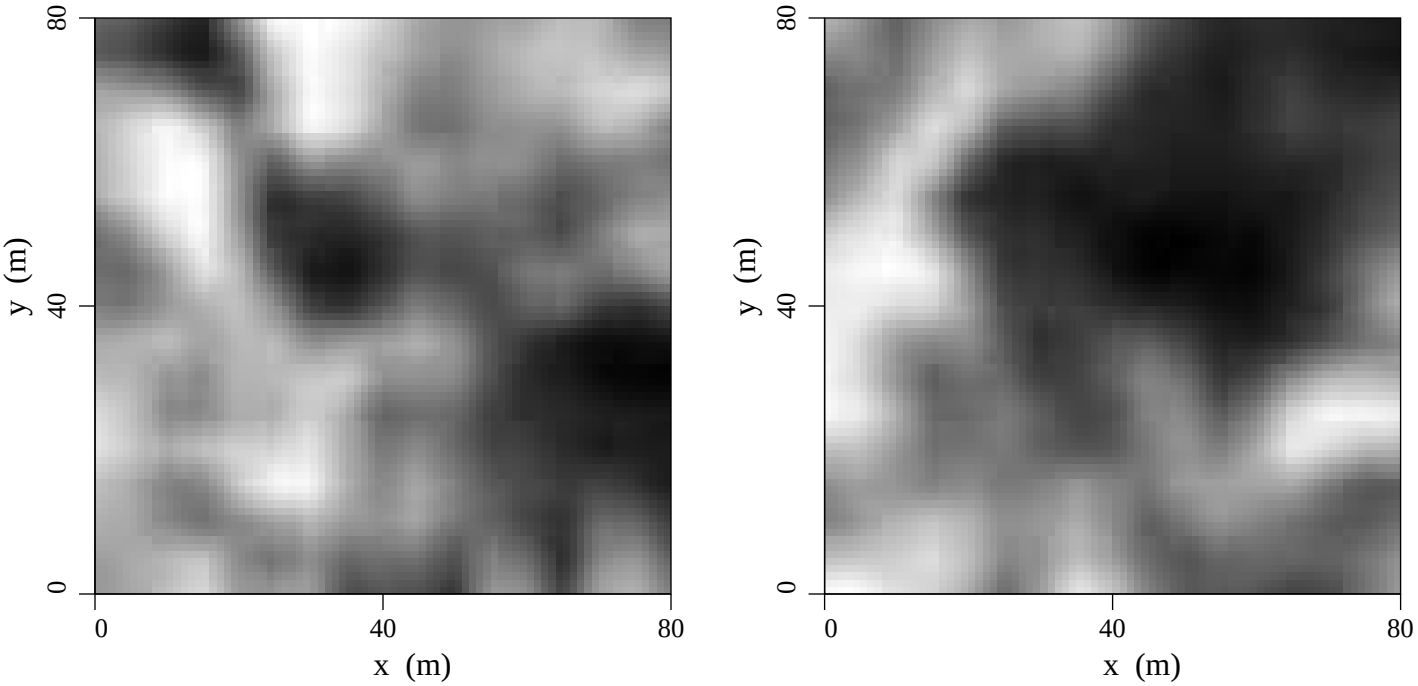

Figure 5. Greyscale maps of the planes having the highest average liquefaction index q drawn from two realizations of the soil mass.

3. MONTE-CARLO ANALYSIS AND RESULTS

The four cases considered are summarized in Table 2. In the following, the first set of simulated ground motions are referred to as Event 1 and the ground motions scaled by a factor of 0.7 as Event 2.

Table 2. Ground motion scaling factors and vertical scales of fluctuation considered in the probabilistic analysis.

Case	Input Motion Scaling Factor	Vert. Scale of Fluctuation (m)	Number of Realizations
1	1.0 (Event 1)	1.0	100
2	1.0 (Event 1)	4.0	100
3	0.7 (Event 2)	1.0	100
4	0.7 (Event 2)	4.0	100

The average depth at which the maximal plane occurs is about 2.7 m for Cases 1 and 3, and about 3.0 m for Cases 2 and 4. Thus it appears that the larger scales of fluctuation result in somewhat lower maximal planes. These results are in basic agreement with the location of liquefied units observed by Holzer *et al.* (1989).

The average excursion area, expressed as a fraction of the total domain area, of the maximal plane exceeding a threshold liquefaction index q, $\bar{A}_q$, is shown in Figure 6. $\bar{A}_q$ is obtained by averaging the A_q values over the 100 realizations for each case. The trend in Figure 6 is evident;

1) the scale of fluctuation has little effect on the average excursion fraction $\bar{A}_q$,
2) the intensity of the input motion has a significant effect on the excursion fractions, as expected. A 30% reduction in input motion intensity reduced the liquefaction index corresponding to $\bar{A}_q$ = 17% from 0.9 to about 0.35, almost a three-fold reduction.

According to Figure 6, only about 20% of the model site had liquefaction indices in excess of 0.9 under event 1. Since an event of this magnitude did result in sand boils and lateral spreading at the Wildlife site, the simulation results suggest that global liquefaction may occur even if only a relatively low percentage of the site is predicted to liquefy. This observation emphasizes the need to rationally quantify the spatial distribution of liquefaction and its effect on global liquefaction risk in future studies.

It appears that the likelihood of global liquefaction due to Event 2 is quite low. To some extent, this is substantiated by the fact that the Wildlife site did not (globally) liquefy during the Elmore Ranch event (M_s = 6.2 compared to the Superstition Hills event, M_s = 6.6) (Keane and Prevost, 1989). Figure 6 suggests a possible approach to the evaluation of liquefaction risk using the knowledge that the Wildlife site is highly liquefiable: determine the average area of the maximal planes which exceed a liquefaction index of 0.9 – global liquefaction risk increases as this area increases. In this particular study (case 1 or 2) only some 15 to 20% of the total area liquefied under this criterion. It is unknown at this time if this proportion of liquefaction is generally sufficient to result in global liquefaction. Such a measure needs to be substantiated and verified through similar studies of other sites and other earthquakes. It nevertheless suggests that, under reasonable assumptions about the site and the earthquake, soil liquefaction can vary significantly over space and only a small fraction need actually liquefy to cause structural damage.

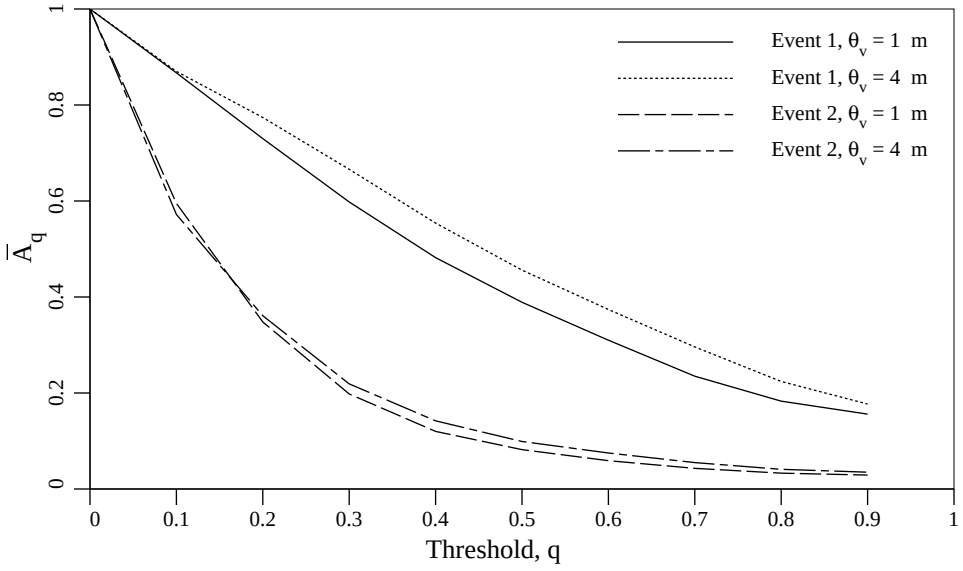

Figure 6. Average fraction of the maximal plane, $\bar{A}_q$, having liquefaction indices in excess of the indicated q thresholds.

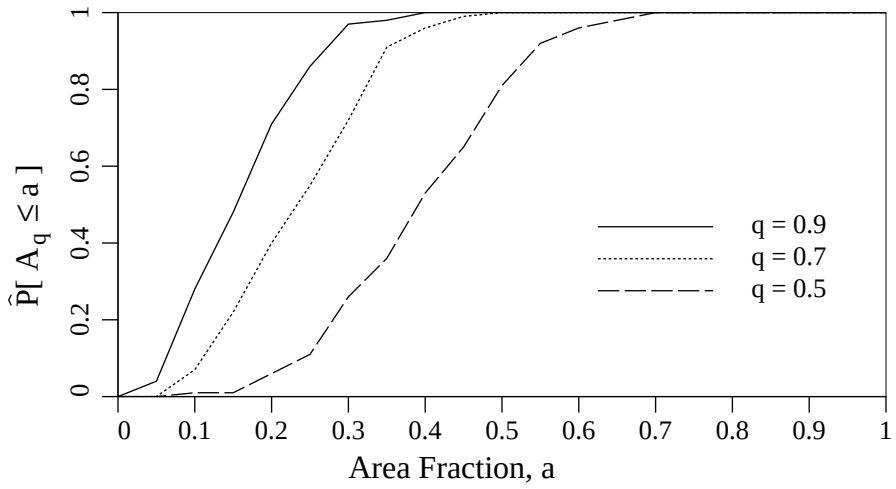

Figure 7. Estimated probability distribution of area fraction with liquefaction index greater than q (for event 1, θ_v = 1 m).

The spatial variability of liquefaction can be quantified in a number of ways; the total area of excursions (exceeding some liquefaction index), the number of isolated excursions, and the degree to which the individual excursions are clustered. Figure 7 shows the estimated probability distribution, $\hat{P}$, of the area fraction having liquefaction indices greater than q for event 1, θ_v = 1.0 m. From this plot it can been seen that, for example, $\hat{P}[A_{0.9} > 0.2] = 1 - 0.7 = 0.3$, that is 30% of realizations have more than 20% of the maximal plane area with liquefaction indices higher than 0.9. Similarly, more than 10% of the maximal plane area effectively liquefies ($q_{ij} \geq 0.9$) with probability 72%.

Figure 8 shows the average number of isolated excursions above the liquefaction index q for each case study and Figure 9 shows the corresponding cluster measure, Ψ, both averaged over 100 realizations. The cluster measure, as defined by Fenton and Vanmarcke (1992), reflects the degree to which excursion regions are clustered. Ψ has value 0 if the excursions are uniformly distributed through the domain and value 1 if they are clumped into a single region or excursion. Both figures exhibit much more pronounced effects due to changes in the scale of fluctuation. The scale of fluctuation θ_v = 4 m (θ_h = 160 m) substantially decreases the average number of excursions and substantially increases the cluster measure. This implies that for the same total area exceeding a certain index q, the regions show higher clustering at higher scales of fluctuation. In turn higher clustering implies a higher likelihood of global liquefaction since there are fewer pockets of 'resistance' within the excursion region. Notice that Event 2 typically has higher mean values of Ψ since it has fewer excursions at high thresholds (a single excursion, or no excursions, corresponds to $\Psi \simeq 1$). The likelihood of liquefaction thus cannot depend on the cluster measure alone; it must also take into consideration the total excursion area above a high threshold.

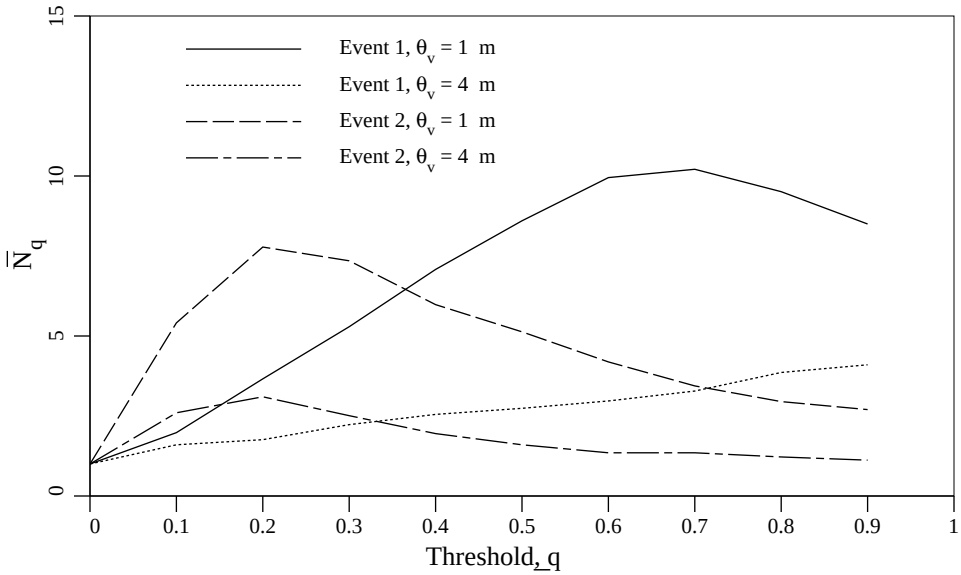

Figure 8. Average number of isolated excursion areas, N_q, where liquefaction indices exceed the threshold q.

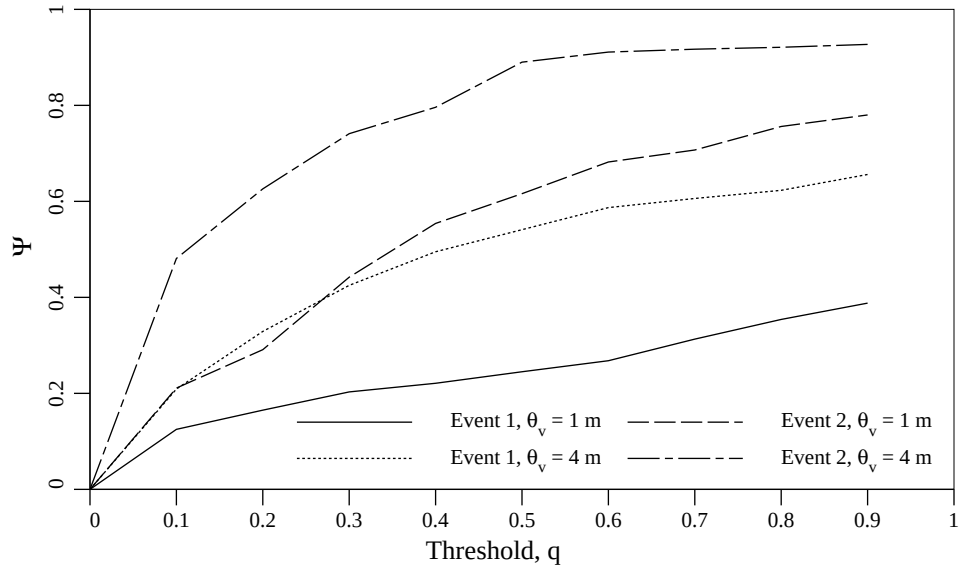

Figure 9. Average cluster measure, Ψ, of isolated excursions where liquefaction indices exceed the threshold q.

4. CONCLUSIONS

It is recognized that the one-dimensional finite element analysis employed in this study cannot capture some of the details of spatial liquefaction, the connection between soil columns being only through their correlated properties and earthquake ground motion. However, the resulting analysis

was tractable at this time (a fully three-dimensional analysis is still prohibitively computationally expensive), allowing the analysis of a sufficient number of realizations for reasonable statistics. It is believed that the major, large scale, features of the spatial distribution of liquefaction initiation are nevertheless captured by the present analysis allowing the following observations to be made.

Perhaps the major observation to be drawn from this study is that (predicted) soil liquefaction shows considerable spatial variability under reasonable assumptions regarding the site and its excitation. The recognition of this spatial variability may significantly advance our understanding and modelling of the phenomenon, allowing the probabilistic assessment of the spatial extent of liquefaction damage. The present study indicated that as little as 15 to 20% of a site which is known to have liquefied was actually predicted to liquefy during the event. Whether or not this the actual fraction of liquefaction at the site is unknown. There is also a possibility of further post-event liquefaction.

Given the fact that the Wildlife site was known to have liquefied during the Superstition Hills event, the following summary of the results of this model study can be made;

1) The spatially random approach to liquefaction analysis enables quantifying the probability of effectively liquefied area fractions or excursions at the site. For example, on the basis of this study, more than 10% of the model site over a plane at about 2.7 m depth was predicted to effectively liquefy ($q \geq 0.9$) with probability 72% during event 1 (θ_v = 1 m), which was modeled after the Superstition Hills event.
2) The likelihood of global liquefaction resulting in loss of lateral stability at the surface appears to be most easily quantified by the total area of the domain whose liquefaction indices exceed some threshold index q^*. In this case study if the threshold index is taken as 0.9, a high likelihood of global liquefaction might be associated with mean total excursion areas A_{q^*} in excess of about 15 to 20% of the total domain area. This measure incorporates the effect of earthquake intensity but needs to be calibrated through other studies and, in time, through fully three-dimensional models.
3) The likelihood of liquefaction can be modified by the cluster measure – as the cluster measure decreases, the liquefied regions become separated by pockets of resistance and the likelihood of global liquefaction at the site decreases. This correction incorporates the effect of scales of fluctuation of the soil properties.

The recognition that liquefaction is a spatially varying phenomenon and the development of techniques to quantify this variability, along with its implications on risk, are important starts in the understanding of global liquefaction failure at a site. The study also illustrates the potential danger in assessing liquefaction risk at a site on the basis of, for example, CPT data collected at a single location. Data from several different locations should be considered so that liquefiable regions can be more closely identified and subsequently modeled in a dynamic structural evaluation.

5. Acknowledgements

Thanks are due to the Natural Sciences and Engineering Research Council of Canada for their financial support under Grant OPG0105445, to the National Science Foundation under Grant ECE–86–11521, and to NCEER under Grant 87–6003. Any opinions, findings, and conclusions and recommendations are those of the authors and do not necessarily reflect the views of the aforementioned organizations.

Appendix I REFERENCES

Asaoko, A. and Grivas, D.A. (1982). Spatial Variability of the Undrained Strength of Clays, *ASCE Journal of Geotechnical Engineering*, **108**(5), pp 743-756.

Bennett, M.J., McLaughlin, P.V., Sarmiento, J.S. and Youd, T.L. (1984). Geotechnical Investigation of Liquefaction Sites, Imperial County, California, United States Department of the Interior Geological Survey, Open-File Report 84-252, Menlo Park, California.

Boissières, H.P. and Vanmarcke, E.H. (1995). Spatial correlation of earthquake ground motion: non-parametric estimation, *Soil Dynamics and Earthquake Engineering*, **14**, pp 23–31.

Chiasson, P., Lafleur, J., Soulié, M. and Law, K.T. (1995). Characterizing spatial variability of a clay by geostatistics, *Canadian Geotechnical Journal*, **32**, pp 1–10.

DeGroot, D.J. and Baecher, G.B. (1993). Estimating autocovariance of in-situ soil properties, *ASCE Journal of Geotechnical Engineering*, **119**(1), pp 147–166.

Fardis, M.N. and Veneziano, D. (Mar. 1982). Probabilistic Analysis of Deposit Liquefaction, *ASCE Journal of Geotechnical Engineering*, **108**(3), pp 395-418.

Fenton, G.A. (1990). Simulation and Analysis of Random Fields, Ph.D. Thesis, Princeton University, Dept. of Civil Engrg. and Op. Res., Princeton, New Jersey.

Fenton, G.A. and Vanmarcke, E.H. (1990). Simulation of Random Fields via Local Average Subdivision, *ASCE Journal of Engineering Mechanics*, **116**(8), pp 1733–1749.

Fenton, G.A. (1994). Error evaluation of three random field generators, *ASCE Journal of Engineering Mechanics*, **120**(12), pp 2478–2497.

Fenton, G.A. and Vanmarcke, E.H. (1992). Simulation-based excursion statistics, *ASCE Journal of Engineering Mechanics*, **118**(6), pp 1129–1145.

Holzer, T.L., Youd, T.L. and Bennett, M.J. (1988). *In situ* Measurement of Pore Pressure Build-Up During Liquefaction, *Proceedings of the 20^{th} Joint Meeting of United States-Japan Panel on Wind and Seismic Effects*, issued by NIST, Jan 1989, pp 118–130.

Holzer, T.L., Youd, T.L. and Hanks, T.C. (1989). Dynamics of liquefaction during the 1987 Superstition Hills, California earthquake, *Science*, **244**, pp 56–59.

Hryciw, R.D., Vitton, S. and Thomann, T.G. (1990). Liquefaction and flow failure during seismic exploration, *ASCE Journal of Geotechnical Engineering*, **116**(12), pp 1881–1899.

Keane, C.M. and Prevost, J.H. (1989). An Analysis of Earthquake Data Observed at the Wildlife Liquefaction Array Site, Imperial County, California, *Proceedings of the Second U.S.-Japan Workshop on Liquefaction, Large Ground Deformations and Their Effects on Lifelines*, Technical Report NCEER-89-0032, Buffalo, NY, pp 176–192.

Lumb, P. (1966). The Variability of Natural Soils, *ASCE Journal of Geotechnical Engineering*, **3**(2), pp 74-97.

Marsily, G. (1985). Spatial Variability of Properties in Porous Media: A Stochastic Approach, in *Advances in Transport Phenomena in Porous Media*, NATO Advanced Study Institute on Fundamentals of Transport Phenomena in Porous Media, Bear, J. and Corapcioglu, M.Y., eds., Dordrecht, Boston, MA, pp 719-769.

Prevost, J.H. (1989). A computer program for nonlinear seismic response analysis, National Center for Earthquake Engineering Research, Technical Report NCEER-89-0025, Buffalo, NY.

Schultze, E. (1971). Frequency distribution and correlation of soil properties, *Proceedings of the First International Conference on Applications of Statistics and Probability to Soil and Structural Engineering*, Hong Kong, Sep 13-16, pp 371–387.

Seed, H.B. (1979). Soil liquefaction and cyclic mobility evaluation for level ground during earthquakes, *ASCE Journal of Geotechnical Engineering*, **105**(GT2), pp 201–255.

Shinozuka, M. and Ohtomo, K. (1989). Spatial Severity of Liquefaction, *Proceedings of the Second U.S.-Japan Workshop on Liquefaction, Large Ground Deformations and Their Effects on Lifelines*, Technical Report NCEER-89-0032, pp 193–206.

Singh, A. and Lee, K.L. (1970). Variability in soil parameters, *Proceedings of the 8th Annual Engineering Geology and Soils Engineering Symposium*, Pocatello, Idaho, Apr 1-3, pp 159–186.

Vanmarcke, E.H. (1984). *Random Fields: Analysis and Synthesis*, The MIT Press, Cambridge, Massachusetts.

Vanmarcke, E.H. (1977). Probabilistic Modeling of Soil Profiles, *ASCE Journal of Geotechnical Engineering*, **103**(GT11), pp 1227–1246.

Vanmarcke, E.H., Heredia-Zavoni, E. and Fenton, G.A. (1993). Conditional simulation of spatially correlated earthquake ground motion, *ASCE Journal of Engineering Mechanics*, **119**(11), pp 2333–2352.

Appendix II NOTATION

The following symbols are used in this paper:

A = total area of the site model

A_q = excursion area fraction of the maximal plane where liquefaction indices exceed q

$\bar{A}_q$ = average excursion area fraction of the maximal plane where liquefaction indices exceed q

a, b = constants

$B(\cdot)$ = spatial covariance function

c = shear wave velocity

E = solid phase elastic modulus

$f_X(x)$ = probability density function of random variable X

$G(\cdot)$ = one-sided marginal pseudo-evolutionary spectral density function

h = total depth of soil column

$I_A(a)$ = indicator function, = 1 if $a > 0$, = 0 otherwise

k = permeability

L = liquefaction risk

M_s = surface wave earthquake magnitude

$\bar{N}_q$ = average number of isolated excursions in the maximal plane where liquefaction indices exceed q

n = porosity

n_c = number of 1-D columns used in the model

$\hat{P}$ = estimated probability distribution

q = liquefaction index

q_i = liquefaction index of element i, = u_i/σ'_{oi}

$q_{ij}(t_l)$ = liquefaction index of element i in column j at time t_ℓ

q^* = threshold liquefaction index

$Q_{i\ell}$ = i'th layer average liquefaction index at time t_ℓ

$\mathcal{Q}$ = vertically averaged liquefaction index

s = dimensionless parameter of space-frequency correlation function

t_ℓ = time of the ℓ'th time step

$\mathcal{T}_i$ = transformation function of the i'th property

$u(z)$ = pore water pressure at depth z

u_i = pore water pressure in element i

$U(\underset{\sim}{x})$ = spatially random material property at the point $\underset{\sim}{x}$

$\underset{\sim}{x}$ = spatial point, having components (x, y, z), z measured vertically from surface

$Y(\underset{\sim}{x})$ = Gaussian random field

$Z_i(\underset{\sim}{x})$ = standard Gaussian random field corresponding to property i

ΔA_j = cross-sectional area of column j

Φ = dilation angle

ϕ = friction angle

η_i = liquefied fraction of element i

$\eta(z)$ = sample liquefied fraction at depth z

μ_i = mean of property i

$\mu_{\ln i}$ = mean of the logarithm of property i

ν = Poisson's ratio

θ_v = scale of fluctuation in the vertical direction

θ_h = scale of fluctuation in the horizontal directions

ρ_s = solid phase mass density

ρ_w = fluid phase mass density

$\rho(\cdot)$ = correlation function

σ_i = standard deviation of property i

$\sigma_{\ln i}$ = standard deviation of the logarithm of property i

σ'_{oi} = initial vertical effective stress in element i

$\sigma'_o(z)$ = initial vertical effective stress at depth z

$\underset{\sim}{\tau}$ = lag vector, having components (τ_1, τ_2, τ_3), τ_3 measured vertically

ω = frequency

Ψ = cluster measure